


Graphene oxide as solid-state electron mediator enhanced photocatalytic activities of GO-Ag₃PO₄/Bi₂O₃ Z-scheme photocatalyst efficiently by visible-light driven

Jixiang Wang, Hongqiang Shen, Xiaohui Dai, Chunmei Li, Weidong Shi & Yongsheng Yan

To cite this article: Jixiang Wang, Hongqiang Shen, Xiaohui Dai, Chunmei Li, Weidong Shi & Yongsheng Yan (2018): Graphene oxide as solid-state electron mediator enhanced photocatalytic activities of GO-Ag₃PO₄/Bi₂O₃ Z-scheme photocatalyst efficiently by visible-light driven, Materials Technology, DOI: [10.1080/10667857.2018.1455385](https://doi.org/10.1080/10667857.2018.1455385)

To link to this article: <https://doi.org/10.1080/10667857.2018.1455385>

 View supplementary material 

 Published online: 02 Apr 2018.

 Submit your article to this journal 

 View related articles 

 View Crossmark data 



Graphene oxide as solid-state electron mediator enhanced photocatalytic activities of GO-Ag₃PO₄/Bi₂O₃ Z-scheme photocatalyst efficiently by visible-light driven

Jixiang Wang^a, Hongqiang Shen^b, Xiaohui Dai^a, Chunmei Li^c, Weidong Shi^a and Yongsheng Yan^a

^aSchool of Chemistry and Chemical Engineering, Jiangsu University, Zhenjiang, People's Republic of China; ^bSchool of Materials Science and Engineering, Jiangsu University, Zhenjiang, People's Republic of China; ^cInstitute of Green Chemistry and Chemical Technology, Jiangsu University, Zhenjiang, People's Republic of China

ABSTRACT

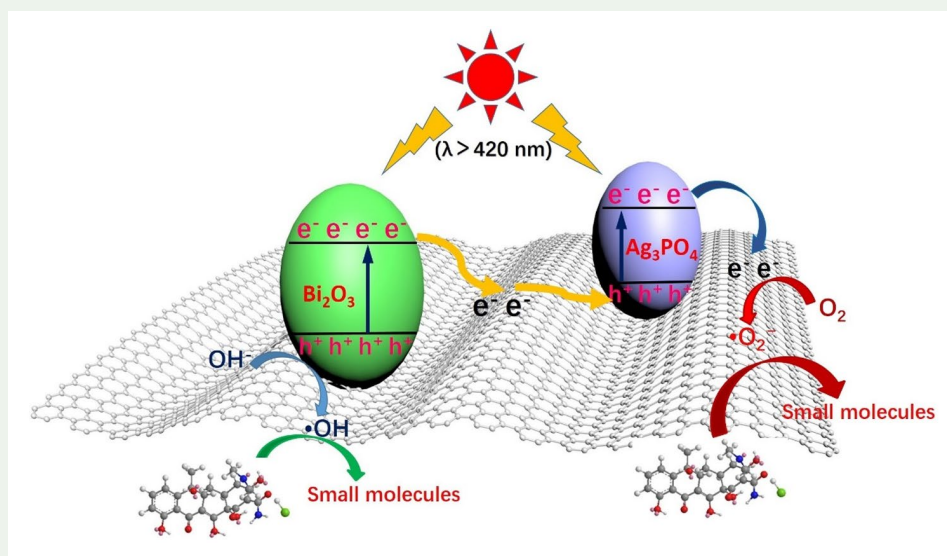
The photocatalytic technology provides a simple and effective strategy for the ever-increasing environmental and energy problem. In this work, we put forward a practical method to facilitate effectively the separation of photogenerated electrons and holes by addition of graphene oxide in Ag₃PO₄ and Bi₂O₃ nanocrystals semiconductor composite. Compared with GO-single component, the three-component GO-Ag₃PO₄/Bi₂O₃ composites with the optimum Ag₃PO₄/Bi₂O₃ ratio (6:4) and content of GO (6 wt-%) presented a further improvement on the photodegradation of tetracycline by visible light irradiation driven. GO served as a medium is used to effectively transfer of the photogenerated electrons from the conduction band Bi₂O₃ of to the valence band of Ag₃PO₄, the Z-Scheme photocatalytic degradation mechanism was proposed. Our work provides an effective method for development of pragmatic photocatalyst in present environmental pollution, energy problems and other related fields.

ARTICLE HISTORY

Received 28 August 2017
Accepted 16 March 2018

KEYWORDS

Z-scheme; graphene; photocatalytic; tetracycline; Ag₃PO₄



Introduction

Semiconductor nanomaterials have become a hot topic in the world to remove environmental pollutants and solve the energy crisis [1–3]. Common semiconductors such as TiO₂ [4], Ag₃PO₄ [5] and BiVO₄ [6] have been reported that their photocatalytic properties are better previously. However, pristine Ag₃PO₄ still express low charge transport properties, lead to poor photocatalytic activity, the photocatalytic efficiency of visible light is curbed. In order to promote the separation of photo-generated electrons and holes, many scientific research

workers improved the photocatalytic capability of Ag₃PO₄, mainly including morphological optimization and heterojunctions manufacturing. Ag₃PO₄ has been compound with many semiconductor and constructed heterostructures photocatalyst [7]. Liu et al. [8] prepared Ag₃PO₄@g-C₃N₄ core@shell composites via ultrasonication/chemisorption method, degrading 97% MB after irradiation for 30 min.

Graphene oxide is a new carbon material with a planar honeycomb lattice structure by SP² after hybridization of carbon atoms, due to its unique two-dimensional

CONTACT Weidong Shi swd1978@ujs.edu.cn; Yongsheng Yan yys@mail.ujs.edu.cn

Supplemental data for this article can be accessed at <https://doi.org/10.1080/10667857.2018.1455385>.

© 2018 Informa UK Limited, trading as Taylor & Francis Group

structure so that it has the characteristics of large surface area, excellent electrical conductivity and chemical stability etc. [9,10]. On account of the characteristics, graphene has been used to form a large number of semiconductor composite materials [11], the photocatalytic activity of the composite material compared to a single semiconductor has been greatly improved [12–14]. Such as, Yang et al. [15] prepared a Ag_3PO_4 -graphene (Ag_3PO_4 -GO) photocatalyst by a facile and effective hydrothermal method, and improve the photocatalytic performance under visible light. Although, the addition of graphene can well improve the photocatalytic properties, but the oxidation ability of Ag_3PO_4 valence band is not high, can not produce more hydroxyl radicals, hydroxyl radicals plays an important role in the photocatalytic reaction, this problem is ignored by most of Ag_3PO_4 graphene based composite.

Bismuth oxide ($\alpha\text{-Bi}_2\text{O}_3$) has been widely studied in many visible light photocatalysts due to its narrow band gap, low toxicity and low chemical stability [16–18]. In particular, its high valence band position determines its strong oxidation ability, which makes it become a potential visible light responsive photocatalytic material in wastewater treatment applications [19]. Therefore, Bi_2O_3 was added to the Ag_3PO_4 composite to form a heterogeneous structure to enhance the oxidation capacity of the complex in the valence band position. Ding et al. fabricated facile and effective $\text{Ag}_3\text{PO}_4/\text{Bi}_2\text{O}_3$ hierarchical heterostructures with co-precipitation hydrothermal method. $\text{Ag}_3\text{PO}_4/\text{Bi}_2\text{O}_3$ photocatalyst was provided with obviously enhanced photocatalytic properties and excellent performance in degradation dyestuff under visible light irradiation. In order to improve the photocatalytic activity, promote the separation of photogenerated electrons and holes, and increase the active species in the degradation system, Hence, it is necessary to explore a new approach to solve these problems.

Z-scheme systems has attracted more and more attention because of its excellent redox ability and photocatalytic performance [20]. Compared with the conventional heterojunction photocatalytic systems, the Z photocatalytic systems not only maintains the high electron transfer efficiency, but also makes the best use of the optimal redox potential and also ensures the rapid separation in both semiconductors [21–23]. This systems is inspired by natural photosynthesis, the previously reported Z-scheme photocatalytic systems is composed of two different semiconductors and a shuttle redox mediator, for example $\text{Fe}^{3+}/\text{Fe}^{2+}$, IO_3^-/I^- and so on. In the past few years, various solid electron conducting medium have been used in place of the shuttle redox mediator to construct Z-scheme photocatalytic systems [24,25]. Cui et al. [26] prepared a $\text{Ag}_3\text{PO}_4/\text{RGO}/\text{Ag}$ photocatalyst with excellent photocatalytic activity and light corrosion resistance, the rhodamine B can be completely

oxidized and degraded within 30 min under visible light irradiation, which acts up on Z-scheme electron transfer reaction mechanisms. Shi et al. [27] add BiVO_4 and Bi_2O_3 into the ethanol solution of graphene oxide, and then developed a three-component Z-scheme nano-heterostructure systems of the $\text{BiVO}_4/\text{RGO}/\text{Bi}_2\text{O}_3$ via the photodeposition method. The sample has a higher photocatalytic activity than that of the single semiconductor BiVO_4 and Bi_2O_3 , and the degradation efficiency of toluene can reach 95.6%. The Z-scheme systems could generate superoxide anion and hydroxyl radicals, and showed the enhanced photostability and photoactivity under visible-light irradiation.

In this work, we used graphene oxide as electronic conduction medium, introducing different semiconductor photocatalysts, and a series of photocatalytic composite material $\text{GO-Ag}_3\text{PO}_4/\text{Bi}_2\text{O}_3$ were synthesized by a simple and efficiency method, then make up Z-scheme photocatalytic systems. GO acts as a solid medium to transfer electrons from Bi_2O_3 to Ag_3PO_4 in this Z-scheme systems, and the utilization of the dominant energy band can be greatly improved by the construction of the Z-scheme photocatalytic systems. Herein, the photocatalytic activity to the degradation for tetracycline were systematically studied via Ag_3PO_4 , Bi_2O_3 mass ratio and the content of graphene oxide. $\text{GO-Ag}_3\text{PO}_4/\text{Bi}_2\text{O}_3$ photocatalyst composites exhibited better catalytic activity than $\text{GO-Ag}_3\text{PO}_4$ or $\text{GO-Bi}_2\text{O}_3$ under visible light.

Experimental

Materials

AgNO_3 , Na_2HPO_4 , HCl , HNO_3 , H_2SO_4 , NaOH , KMnO_4 , P_2O_5 , $\text{K}_2\text{S}_2\text{O}_8$, Flake graphite, $\text{C}_2\text{H}_5\text{OH}$, Bi_2O_3 were obtained from Sinopharm (Beijing, China). H_2O_2 was purchased from Aladdin (Shanghai, China). All chemicals and solvents used were prepared from analytical grade. MiniQ water was used throughout the experiments.

Instruments

The X-ray diffraction (XRD) patterns were obtained with a D/MAX-2500 X-ray powder diffractometer with Cu K α radiation and a scan rate of 7° min^{-1} for 2θ measurements over the range of $5\text{--}80^\circ$. The morphologies of the products were characterized using a scanning electron microscope (JEOL JSM-7001F) equipped with an energy-dispersive X-ray spectroscopy (EDS) operated at an acceleration voltage of 10 kV. The transmission electron microscopy (TEM) and high-resolution TEM (HRTEM) were carried out with a JEM-2100 electron microscope (JEOL, Japan). Raman spectra were recorded at room temperature using a micro Raman spectrometer (Renishaw Invia) in a backscattering geometry with a 532 nm laser as an excitation

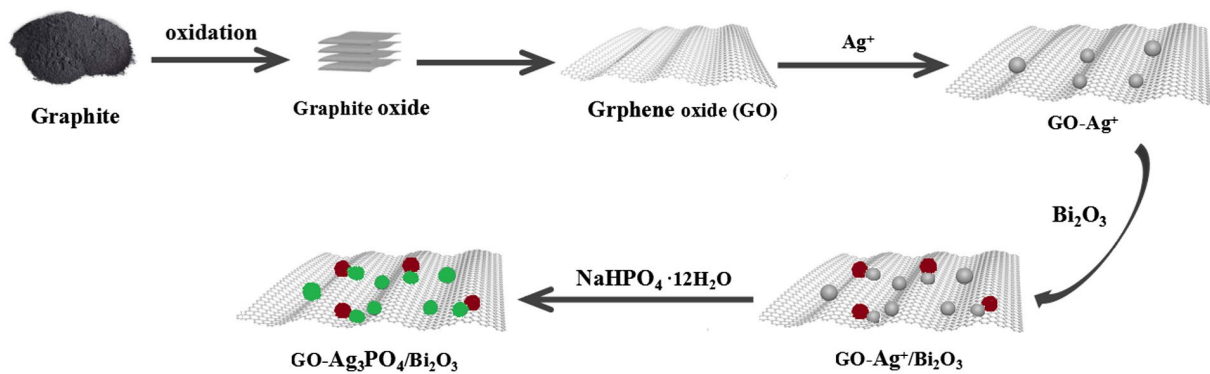


Figure 1. Schematic illustrating the synthesis of GO-Ag₃PO₄/Bi₂O₃ photocatalysts.

source. The UV–vis diffused reflectance spectra (DRS) of the samples were acquired using an UV–vis spectrophotometer (UV-2450, Shimadzu, Japan). The photoluminescence (PL) spectra fluorescence lifetime (FL) of samples were recorded on a Perkin-Elmer LS 55 at room temperature using a fluorescence spectrophotometer. The X-ray photoelectron spectroscopy (XPS) was conducted using a Thermo ESCALAB 250X (America) electron spectrometer using 150 W Al K α X-ray sources. The electrochemical impedance spectroscopy (EIS) was characterized by an electrochemical system (CHI-7601, China).

Synthesis of graphene oxide (GO)

GO was synthesized via a modified Hummer's method. Typically, Flake graphite (3 g), P₂O₅ (2.5 g) and K₂S₂O₈ (2.5 g) were added into 12 mL 98% H₂SO₄, and the mixture was stirred at 353 K for 2 h by magnetic stirring apparatus continuously. Then, the treated mixture was diluted with distilled water (500 mL) and filtered under vacuum. During filtration process, distilled water was added slowly to the above mixture to remove the residual acid. Finally, the obtained product was dried at 323 K overnight.

The pre-oxidized graphite solid was put into concentrated sulfuric acid (120 ml) and stirred under ice bath conditions. Then, KMnO₄ (15 g) was added into the above mixture solution, the solution changed to dark green. Then, the dark green solution was stirred at 308 K for 2 h in ice bath condition. After that, distilled water (250 mL) and 30% H₂O₂ (20 mL) was slowly added into the suspended mixture one after another. The obtained yellow solution was filtered and washed with dilute hydrochloric acid solution (10 wt-%) repeatedly, in order to remove the metal ions. Finally, the product (GO) was dried by vacuum drying oven for 24 h under 333 K.

Synthesis of GO-Ag₃PO₄/Bi₂O₃ photocatalysts

GO (50 mg) was ultrasonic dispersed in distilled solution (20 mL) for 2 h. Then, AgNO₃ (0.366 g) was added to the mixture solution and stirred by magnetic stirring apparatus continuously for 30 min. After the pH of the mixture

was slowly adjusted to 8 with 6 M NaOH solution. Then Bi₂O₃ (0.2 g) was also added in the mixture solution and stirred for 45 min constantly, upon Na₂HPO₄ (0.6 g) was added in the mixture and stirred for 30 min again. The resultant was separated and washed several times with MiniQ water and ethanol, and dried at 333 K with a vacuum oven for one night. Because that m(Ag₃PO₄):m(Bi₂O₃) is 6:4 and the amount ratio of graphene is 6 wt-%, so the product was marked as GO-6/4. For comparison, the different complexes of the GO-Ag₃PO₄/Bi₂O₃ photocatalyst (GO-2/8, GO-4/6, GO-8/2) were synthesized as the same as before, the preparation process was illustrated in Figure 1. The added different content of GO in the GO-Ag₃PO₄/Bi₂O₃ hybrid materials were GO-1, GO-3, GO-6, GO-9, GO-12 wt-% respectively.

Photocatalytic experiments

Tetracycline (TC) as a toxic organic pollutant was used to investigate the photocatalytic activity of the GO-Ag₃PO₄/Bi₂O₃ composites under visible-light irradiation. 50.0 mg of photocatalyst was ultrasonic dispersed in 100 mL TC solution (20 mg/L) in a special glass bottle. In order to avoid the influence of adsorption on the photocatalyst surface to TC during the test, the suspension was constantly stirred in the dark for 40 min to achieve absorption-desorption equilibrium. After that, the suspension (5 mL) was sampled and separated by centrifuge before visible-light illumination, whose concentration and absorbance were denoted by C₀ and A₀. Afterwards, the suspension was irradiated using a 300 W xenon lamp with UV cut-off filters and was kept at 298 K by water-cooling device. The sampling and centrifugation processes were repeated every 10 min. The concentration of the solution could be calculated with formula (C/C₀ = A/A₀).

Results and discussion

Characterization of as-prepared samples

The crystal structures and phase data for the composite photocatalysts were characterized by XRD. Figure 2(a) shows the XRD patterns of GO-Ag₃PO₄/Bi₂O₃,

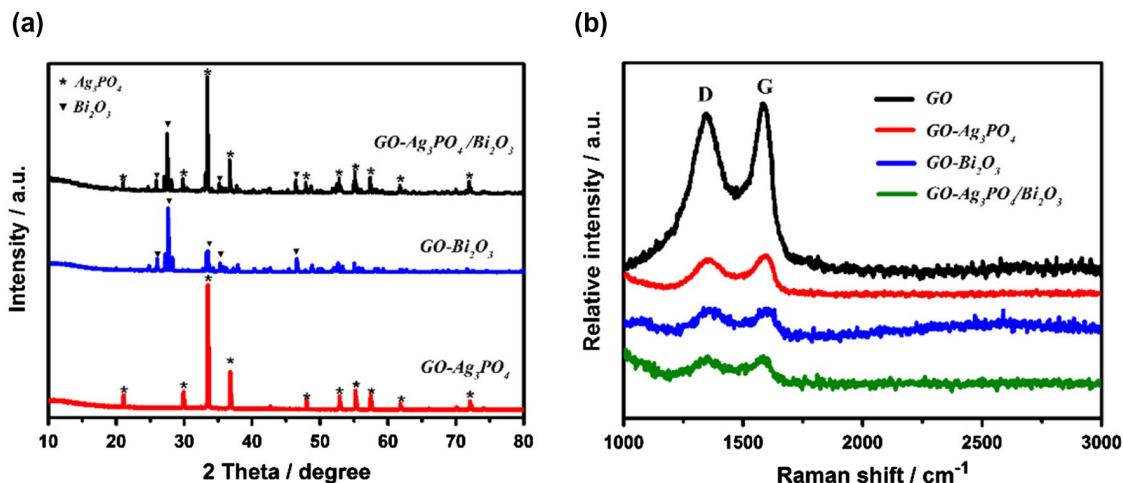


Figure 2. (a) XRD patterns of GO- $\text{Ag}_3\text{PO}_4/\text{Bi}_2\text{O}_3$, GO- Bi_2O_3 and GO- Ag_3PO_4 . (b) Raman spectrum of GO, GO- Ag_3PO_4 , GO- Bi_2O_3 and GO- $\text{Ag}_3\text{PO}_4/\text{Bi}_2\text{O}_3$.

GO- Bi_2O_3 and GO- Ag_3PO_4 , respectively. The diffraction peaks of GO- Ag_3PO_4 at 20.9° , 29.8° , 33.4° , 36.7° , 47.9° , 52.8° , 55.2° , 57.5° , 61.8° and 72.1° were attributed to the (1 1 0), (2 0 0), (2 1 0), (2 1 1), (3 1 0), (2 2 2), (3 2 0), (3 2 1), (4 0 0) and (4 2 1) crystal planes of Ag_3PO_4 , corresponding to JCPDS (74-1876) [28]. The major diffraction peaks of GO- Bi_2O_3 at 25.8° , 27.4° , 33.1° , 35.0° and 46.3° can be identified as the (0 0 2), (-1 2 1), (-2 0 2), (-2 1 2) and (0 4 1) crystal planes of $\alpha\text{-Bi}_2\text{O}_3$ (JCPDS(71-2274)) [29]. The GO- $\text{Ag}_3\text{PO}_4/\text{Bi}_2\text{O}_3$ composite presents the same peaks in agreement with Ag_3PO_4 and $\alpha\text{-Bi}_2\text{O}_3$. Due to the strong intensities of Ag_3PO_4 and Bi_2O_3 patterns, the XRD pattern obtained by reduction of graphene oxide cannot be distinguished, due to its low quantity and poor crystallinity.

In the graphene based photocatalytic systems, successful reduction of GO to rGO plays a key role in the photocatalytic activity. The existence of GO in GO- $\text{Ag}_3\text{PO}_4/\text{Bi}_2\text{O}_3$ composites could be proved by Raman spectroscopy, which could also further confirm the reduction of GO during mixing reaction. The Raman spectra of different samples in Figure 2(b) contain two distinct peaks at ~ 1347 and ~ 1584 cm^{-1} , which can be assigned to the D and G bands from the vibrations of sp^3 and sp^2 carbon atoms in a graphitic 2D planar structure, respectively [30–32]. The sp^2 hybridized carbon had higher degree of oxidation than the sp^3 , so the intensity ratio of D/G was used to reflect the reduction degree of GO [33]. The intensity ratio of ID/IG is calculated to estimate the reduction degree of the graphene oxide. EDS spectrum from the Figure S1 give the signals of C, O, P, Ag and Bi elements in the GO- $\text{Ag}_3\text{PO}_4/\text{Bi}_2\text{O}_3$ (GO50-6/4) photocatalysts, which proved that the as-prepared sample was GO- $\text{Ag}_3\text{PO}_4/\text{Bi}_2\text{O}_3$ composite.

Furthermore, XPS spectra were carried out to investigate the elemental composition, chemical state, mold,

constitute and properties of functional groups involved of the GO- $\text{Ag}_3\text{PO}_4/\text{Bi}_2\text{O}_3$ composite. As shown in Figure 3(a), the survey XPS spectra of the three-phase composite (GO- $\text{Ag}_3\text{PO}_4/\text{Bi}_2\text{O}_3$) exhibit including Ag, Bi, P, O and C elements. The high-resolution scanning XPS spectra (Figure 3(b)) reveal that the binding energies of Ag $3d_{5/2}$ and Ag $3d_{3/2}$ are located at 367.8 and 373.8 eV, respectively, suggesting that Ag (I) exists in the GO- $\text{Ag}_3\text{PO}_4/\text{Bi}_2\text{O}_3$ composites [34]. In Figure 3(v), there were two peaks with the binding energies of 159.7 and 164.40 eV corresponding to Bi $4f_{7/2}$ and Bi $4f_{5/2}$, which implied that bismuth element exists in the form of Bi(III) without formation of elemental bismuth in the alkaline environment [35]. The binding energy of 132.8 eV associated with P2P peaks (Figure 3(d)) and the binding energy of 530.7 eV associated with O 1s peaks are observed (Figure 3(e)), indicating the formation of Ag_3PO_4 and Bi_2O_3 . Moreover, the peak at 284.78 eV in the high-resolution C 1s spectroscopy display in Figure 3(f) is attributed to sp^2 hybridized non-oxygenated ring carbon atoms (C–C). In addition, the other peaks at 286.38 and 288.78 eV were oxygen-containing epoxy/hydroxyl groups (C–O) and carbonyls (C=O), respectively [25,34,36]. The weak peaks of C–C and C=O give a circumstantial evidence for the reduction of GO.

The morphology and superficial microstructure of GO- $\text{Ag}_3\text{PO}_4/\text{Bi}_2\text{O}_3$ photocatalyst was characterized by TEM and HRTEM. As shown in Figure 4(a), the Ag_3PO_4 and Bi_2O_3 nanoparticles with different morphologies irregularly distributed on the surface of GO, which display typical fold, high surface area and ultra-thin nano layer morphology. As can be seen from Figure 4(b), three phase microstructure/nanostructure $\text{Ag}_3\text{PO}_4/\text{Bi}_2\text{O}_3/\text{GO}$ composite. It is clearly reveal that the edge of graphene can also be observed and microsized Ag_3PO_4 particles and Bi_2O_3 nanoparticles grow on the surface of GO, indicating that the Bi_2O_3

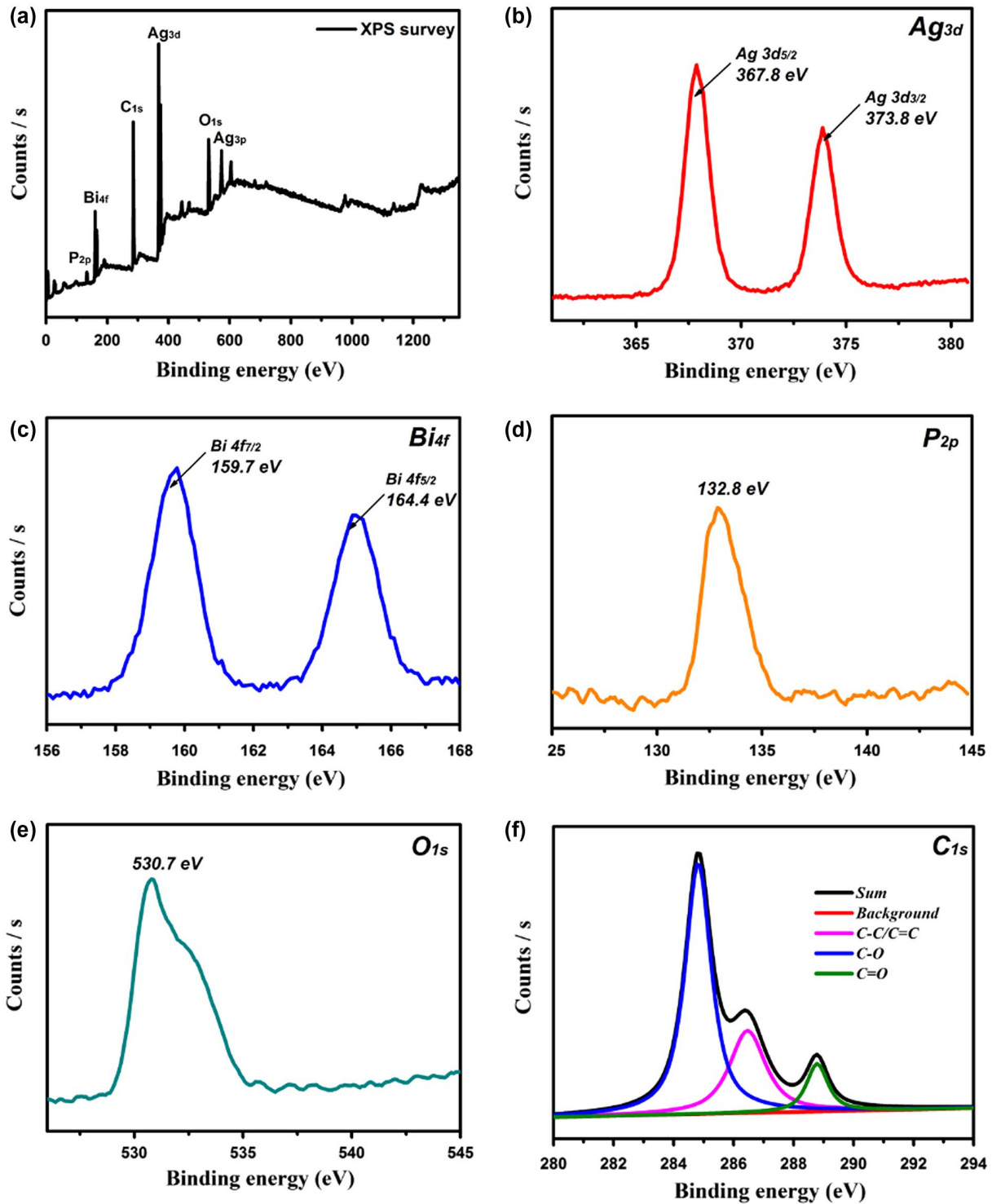


Figure 3. (a) XPS spectrum of GO- $\text{Ag}_3\text{PO}_4/\text{Bi}_2\text{O}_3$, (b) high-resolution scanning XPS of Ag 3d, (c) high-resolution scanning XPS of Bi 4f, (d) high-resolution scanning XPS of P 2p, (e) high-resolution scanning XPS of O 1s, and high-resolution core level XPS spectrum of C 1s of the GO- $\text{Ag}_3\text{PO}_4/\text{Bi}_2\text{O}_3$ nanocomposites.

and Ag_3PO_4 nanoparticles have been firmly loaded on the surface of GO via a mixing method. Further, the HRTEM image (Figure 4(c)) displays the lattice fringe with lattice spacing of 0.268 nm, corresponding to the (210) lattice planes of Ag_3PO_4 (JCPDS 74-1876). And the HRTEM image in Figure 4(d) displays the lattice fringe with lattice spacing of 0.325 nm, which was ascribed to the (121) lattice planes of Bi_2O_3 (JCPDS

71-2274). Figure 4(e)–(h) show the STEM image and the elemental distribution of the GO- $\text{Ag}_3\text{PO}_4/\text{Bi}_2\text{O}_3$ composites, demonstrating that the Ag_3PO_4 and Bi_2O_3 nanoparticles are well separated on the GO sheets. The combination of TEM, HRTEM and STEM characterizations confirm that Ag_3PO_4 and Bi_2O_3 nanoparticles have been successfully loaded on the surface of GO and are spatially well separated.

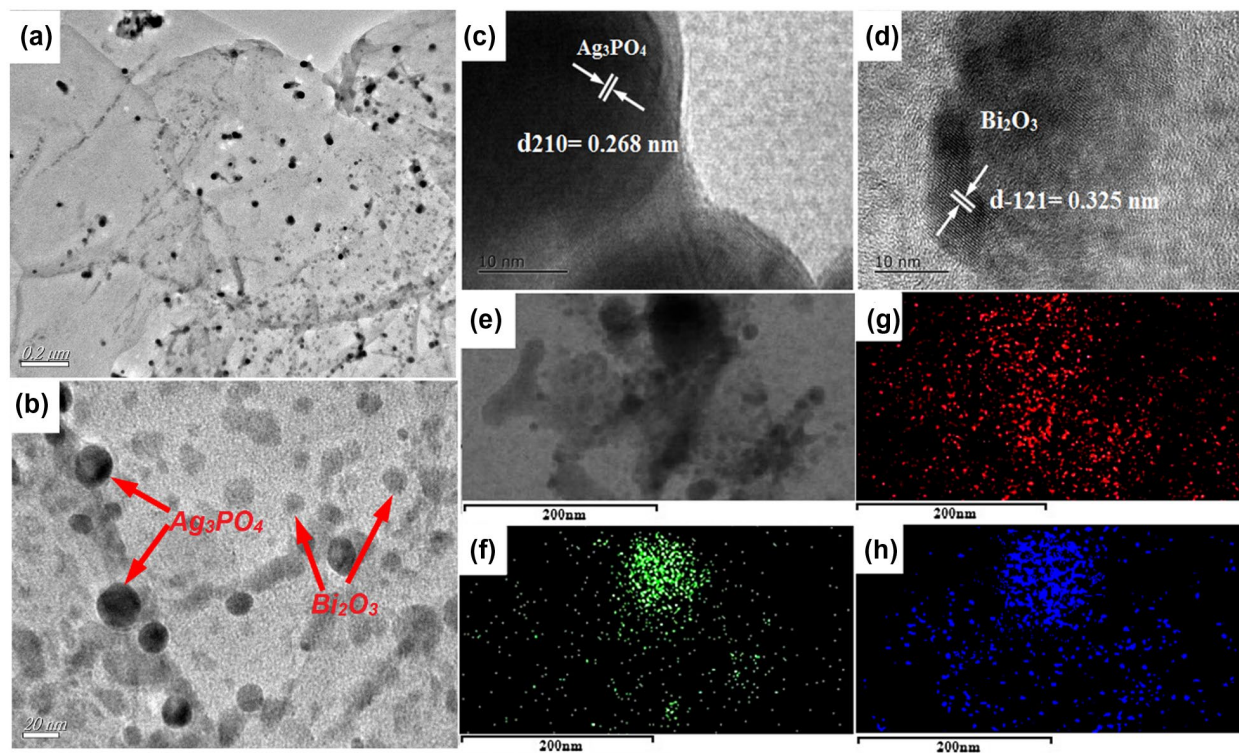


Figure 4. TEM (a, b), HRTEM (c, d) and STEM (e) images of the GO- $\text{Ag}_3\text{PO}_4/\text{Bi}_2\text{O}_3$ composite photocatalysts. Elemental distribution mapping of Ag, Bi and P elements (f, g and h).

According to report, using GO as the precursor for synthetic photocatalysts, the size and shape of the additional semiconductor can be effectively adjusted, owing to the electrostatic interaction. Hence, in order to assess the effect of GO quantity on the morphology of GO- $\text{Ag}_3\text{PO}_4/\text{Bi}_2\text{O}_3$, the SEM images of GO- $\text{Ag}_3\text{PO}_4/\text{Bi}_2\text{O}_3$ (6/4) samples with different amounts ratio of GO were investigated and the results were shown in Figure S2. It is clearly shown in Figure S2a, the aggregates of Ag_3PO_4 and microsized Bi_2O_3 nanoparticles without GO were observed. The introduction of GO substance, resulted in structuring more denser photocatalysts where GO sheets are considered as the support for Ag_3PO_4 and Bi_2O_3 particles. In order to further increase in the GO amount ratio from 1 to 3 wt-% (in Figure S2b&c) led to the generation of Ag_3PO_4 particles with smaller sizes. However, as shown in Figure S2d-f, the use of more than 6 wt-% GO (9, 12 wt-%) as the precursor caused the increase in the diameters of Ag_3PO_4 particles, and the presence of GO (12 wt-%) in the photocatalysts illustrate that the majority of Ag_3PO_4 and Bi_2O_3 particles are coated or wrapped by GO sheets. These illustrate that the negatively charged GO plays a vital role in the nucleation and controlled growth Ag_3PO_4 through electrostatically-driven interactions.

As can be seen from Figure 5, UV-vis absorption spectra reveal the optical absorption properties of synthetic the Ag_3PO_4 , Bi_2O_3 , GO- Ag_3PO_4 , GO- Bi_2O_3 , and GO- $\text{Ag}_3\text{PO}_4/\text{Bi}_2\text{O}_3$ photocatalysts. It is generally accepted that photocatalytic activity is closely related to light absorption capacity. The typical DRS of these

photocatalysts illustrate strong absorption bands with a steep edge in the visible light region. The steep edge announced that visible absorption is caused by band gap transition rather than by non-pure level transition [37]. As shown in Figure 5(a) and (b), all of the synthetic photocatalysts have light reactions from UV region to the visible region, and display high visible-light absorption, which was consistent with the energy band gap. The visible-light absorption edge of the GO- $\text{Ag}_3\text{PO}_4/\text{Bi}_2\text{O}_3$ red shift compare with Ag_3PO_4 and Bi_2O_3 , this could be attributed to GO, which alters the electron interaction and charge balance [38]. The band gap of visible-light absorption can be calculated by the Kubelka-Munk formula, the band gap (E_g) energy of pure Ag_3PO_4 and Bi_2O_3 is calculated to be about 2.23 and 2.64 eV. After addition the GO to the combination of Ag_3PO_4 and Bi_2O_3 , resulted in the red shift and the improvement in visible light absorption range, which might play a significant role in improving photocatalytic performance. Moreover, the relative CB and VB positions of Ag_3PO_4 and Bi_2O_3 were calculated (Table S1).

Evaluation of photocatalytic activity

The photocatalytic activity of as-prepared samples was evaluated by the degradation of organic pollutants with visible-light illumination, in which the tetracycline (TC) was selected as a representative contaminant for its colorless and toxic properties [39]. Different photocatalysts and the effects of the $\text{Ag}_3\text{PO}_4/\text{Bi}_2\text{O}_3$ ratio and the graphene amount were investigated in-depth. The

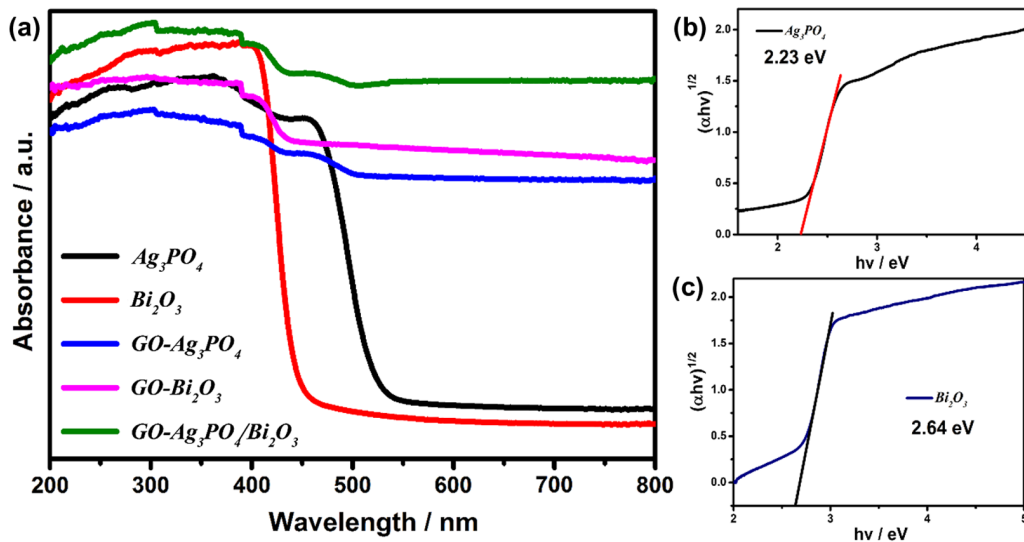


Figure 5. UV-vis diffuse reflection spectra of Ag_3PO_4 , Bi_2O_3 , $GO-Ag_3PO_4$, $GO-Bi_2O_3$, $GO-Ag_3PO_4/Bi_2O_3$.

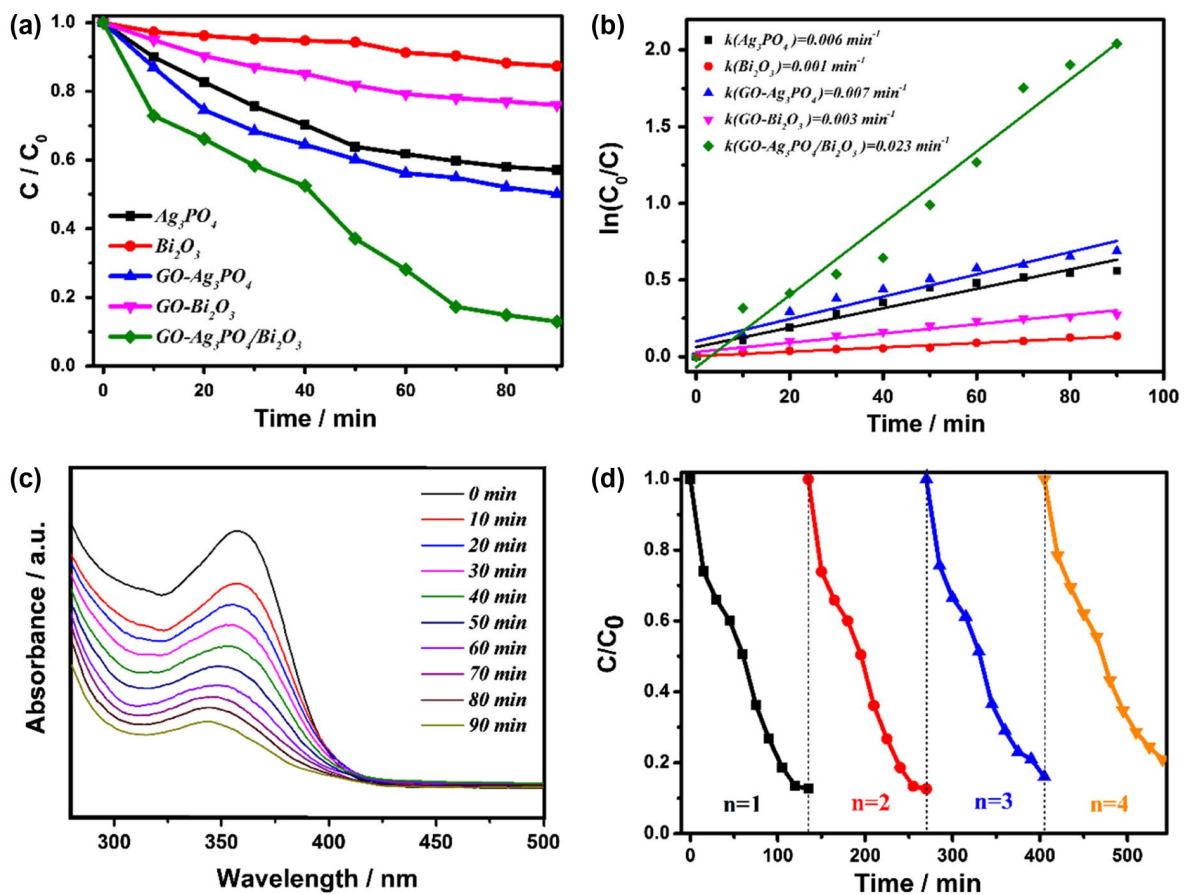


Figure 6. (a) The degradation of TC over the sample with different photocatalysts. (b) plots of $\ln(C_0/C)$ versus irradiation time and rate constant k of TC solutions over different photocatalysts, (c) under visible light ($\lambda > 400$ nm), absorbance variation curves, (d) Repeated experiments of photocatalytic degradation of tetracycline hydrochloride (20 mg/L) by the prepared $GO-Ag_3PO_4/Bi_2O_3$ sample composite.

absorption spectrums of as-prepared photocatalysts were shown in Figure S3a. The solution nearly achieved adsorption equilibrium within 30 min (see details in the Supplementary Material). Figure 6(a) displays the photocatalytic capability of pure Ag_3PO_4 , Bi_2O_3 , $GO-Ag_3PO_4$, $GO-Bi_2O_3$ and $GO-Ag_3PO_4/Bi_2O_3$ via photodegrading

TC. The results indicate that $GO-Ag_3PO_4/Bi_2O_3$ has a higher photocatalytic activity than the other photocatalyst, which further demonstrates that the proper introduction of GO as electron conducting medium will increase the effective utilization of photogenerated electrons. It was clear that the GO played a significant

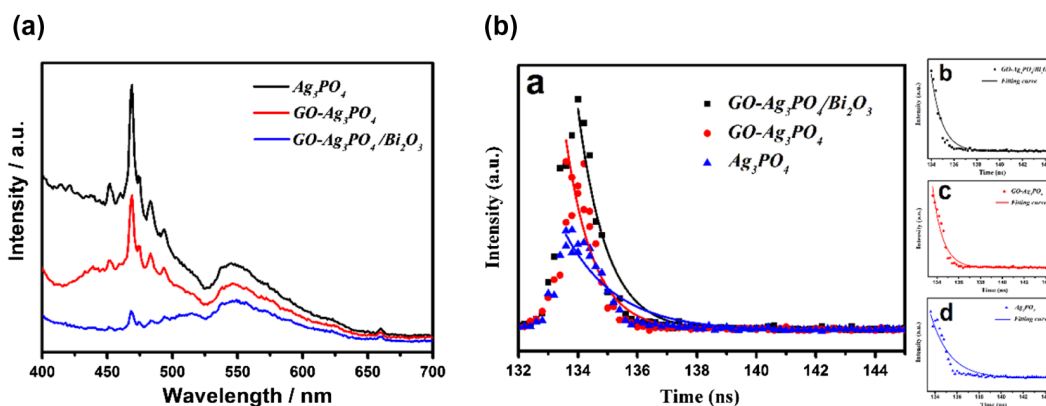


Figure 7. (A) Solid PL emission spectra of Ag_3PO_4 , $\text{GO-Ag}_3\text{PO}_4$, and $\text{GO-Ag}_3\text{PO}_4/\text{Bi}_2\text{O}_3$, excited at 337 nm. 7B(a) FL emission decay (b) of Ag_3PO_4 , $\text{GO-Ag}_3\text{PO}_4$, and $\text{GO-Ag}_3\text{PO}_4/\text{Bi}_2\text{O}_3$, excited at 337 nm, respectively, and the corresponding magnified view of PL decay dynamics (b, c, d).

role in the photocatalytic activities. In addition, compared with two-element photocatalyst, the Z-scheme photocatalyst ($\text{GO-Ag}_3\text{PO}_4/\text{Bi}_2\text{O}_3$) composite has better degradation effect and faster degradation efficiency [40]. The photocatalytic performance of samples over different graphene oxide amount was investigated in Figure S3b. In addition, the photocatalytic performance of samples over different $\text{Ag}_3\text{PO}_4/\text{Bi}_2\text{O}_3$ ratios was also investigated in Figure S3c. The experimental results express The $\text{GO-Ag}_3\text{PO}_4/\text{Bi}_2\text{O}_3$ composite with the optimum $\text{Ag}_3\text{PO}_4/\text{Bi}_2\text{O}_3$ ratio (6:4) and amount ratio of GO (6 wt-%) exhibits a high photocatalytic TC degradation performance (88%) responding to visible light (see details in the Supplementary Material). The TC solution was decomposed more than 85% after 90 min over the $\text{GO-Ag}_3\text{PO}_4/\text{Bi}_2\text{O}_3$ photocatalyst under visible light irradiation. The degradation degree was much higher than that of Ag_3PO_4 , Bi_2O_3 , $\text{GO-Ag}_3\text{PO}_4$ and $\text{GO-Bi}_2\text{O}_3$. The fitting removal rate constant k of $\text{GO-Ag}_3\text{PO}_4/\text{Bi}_2\text{O}_3$ also reached 0.023 min^{-1} (Figure 6(b)), which reached to several times as much as that of other photocatalysts. Besides, the absorbance variations of TC over $\text{GO-Ag}_3\text{PO}_4/\text{Bi}_2\text{O}_3$ are also investigated. Figure 6(c) shows that with the irradiation time increased, the absorbance of TC decreased significantly. After 90 min of visible-light irradiation, there was no significant absorbance peak, this indirectly proved that TC was broken down completely or decomposed into small molecules. Besides, for the photocatalyst, the durability and stability was still significant for practical applications. The reusability of $\text{GO-Ag}_3\text{PO}_4/\text{Bi}_2\text{O}_3$ were further studied by photodegradation TC for five cycles, as shown in Figure 6(d). The photocatalytic efficiency displays a slight decrease due to the photocorrosion occurring on the photocatalyst during the first three photodegradation process. After four cycles, photocatalytic degradation efficiency is unobvious reduced, indicating that the obtained $\text{GO-Ag}_3\text{PO}_4/\text{Bi}_2\text{O}_3$ photocatalyst demonstrates a good recyclability.

Proposed possible photocatalytic mechanism

Photoluminescence, electrochemical impedance and transient photocurrent response analyses

As everyone knows, the fluorescence intensity of semiconductor materials is related to the recombination rate of e^- and h^+ [41,42], it showed a direct proportion relationship. In addition, it illustrated the photocatalytic properties of semiconductor materials is lower. The PL spectra of Ag_3PO_4 , $\text{GO-Ag}_3\text{PO}_4$, and $\text{GO-Ag}_3\text{PO}_4/\text{Bi}_2\text{O}_3$ was shown in Figure 7. The measurement operation was under 337 nm excitation light source in the room temperature, and adding the powder samples with a quartz glass in the device covering. As shown in Figure 7(A), the pure Ag_3PO_4 exhibited an intense emission peak at about 470 nm, which is the highest PL intensity. The introduction of GO and Bi_2O_3 decreases PL intensity of composite photocatalysis, and the peak of $\text{GO-Ag}_3\text{PO}_4/\text{Bi}_2\text{O}_3$ was lower than that of $\text{GO-Ag}_3\text{PO}_4$ composite. For the further examination of charge carrier mobility, the transient fluorescence of Ag_3PO_4 , $\text{GO-Ag}_3\text{PO}_4$, and $\text{GO-Ag}_3\text{PO}_4/\text{Bi}_2\text{O}_3$ excited at 337 nm was introduced and analyzed in Figure 7(B). Corresponding calculation results for fluorescence lifetime of the fitting decay curves of Ag_3PO_4 , $\text{GO-Ag}_3\text{PO}_4$, and $\text{GO-Ag}_3\text{PO}_4/\text{Bi}_2\text{O}_3$ are 1.73, 1.42, and 0.96 ns, respectively (see details in the Supplementary Material). As can be seen from Table S2, the decay time of $\text{GO-Ag}_3\text{PO}_4/\text{Bi}_2\text{O}_3$ is shortest, which has the strongest ability for photogenerated electrons and holes pair separation and effective utilization of the charge carriers. All of these results indicate that the separation of photogenerated electrons and holes has been enhanced by the ternary structure, and enhanced photocatalytic activity.

Electrochemical impedance spectroscopy (EIS) was used to investigate the separation efficiency of electron-hole pairs of the photocatalytic composite material. As is well-known, the arc radius of impedance curve is inversely proportional to the electron-hole separation efficiency and photocatalytic activity. The Nyquist plots

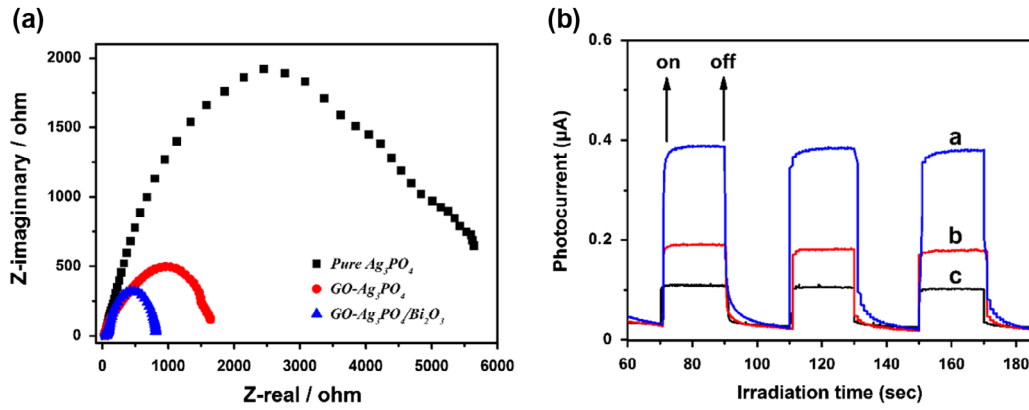


Figure 8. (A) Electrochemical impedance spectroscopy (EIS) of pure Ag_3PO_4 , $\text{GO-Ag}_3\text{PO}_4$ and $\text{GO-Ag}_3\text{PO}_4/\text{Bi}_2\text{O}_3$ (Init E = 0.5 V, $[\text{Na}_2\text{SO}_4] = 0.5 \text{ M}$). (B) Transient photocurrent response of $\text{GO-Ag}_3\text{PO}_4/\text{Bi}_2\text{O}_3$ (a), $\text{GO-Ag}_3\text{PO}_4$ (b) and Ag_3PO_4 (c) nanocomposite in 0.5 M Na_2SO_4 aqueous solution under visible light irradiation.

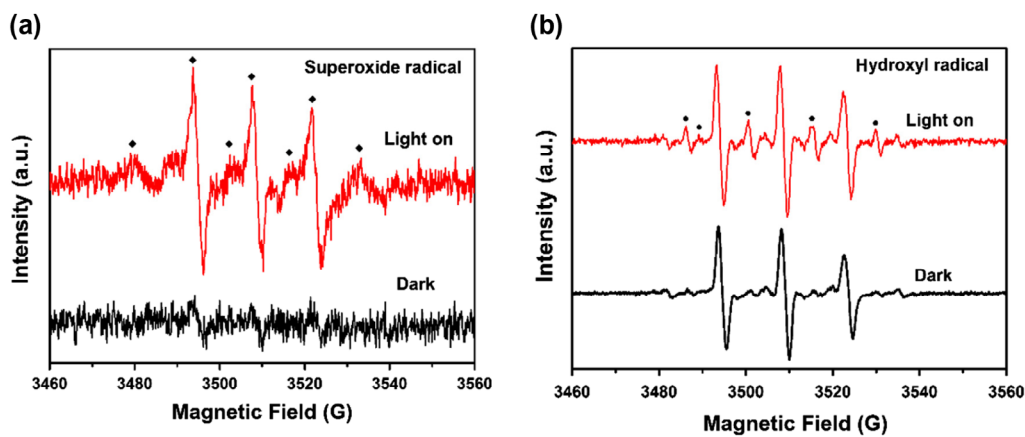


Figure 9. DMPO-ESR spin-trapping spectra of $\text{GO-Ag}_3\text{PO}_4/\text{Bi}_2\text{O}_3$ for detection of (a) superoxide radical ($\bullet\text{O}_2^-$) and (b) hydroxyl radical ($\bullet\text{OH}$).

of pure Ag_3PO_4 , $\text{GO-Ag}_3\text{PO}_4$ and $\text{GO-Ag}_3\text{PO}_4/\text{Bi}_2\text{O}_3$ was shown in Fig. 8. The impedance spectra are strongly influenced by the modification treatment, and the arc radius of the Nyquist plot of the obtained Ag_3PO_4 is larger than that of $\text{GO-Ag}_3\text{PO}_4$ and $\text{GO-Ag}_3\text{PO}_4/\text{Bi}_2\text{O}_3$, suggesting that the modification with GO has changed the charge separation efficiency at the electrode interface.

The fluorescence lifetime of the electrons produced by this light energy can be obtained by transient photocurrent measurements [43,44]. Figure 8(B) shows the transient photocurrent responses of $\text{GO-Ag}_3\text{PO}_4/\text{Bi}_2\text{O}_3$ (a) $\text{Ag}_3\text{PO}_4/\text{Bi}_2\text{O}_3$ (b) and Ag_3PO_4 (c), the photocurrent response was detected by using the visible-light on-off with intermittent time 20 s. This indicates that with the addition of GO, photocurrent current-potential of $\text{GO-Ag}_3\text{PO}_4/\text{Bi}_2\text{O}_3$ photocatalytic composite material increased significantly under visible-light, and as soon as the light is switched off, the photocurrent is reduced to zero. It is clearly shown in Figure 8(B), $\text{GO-Ag}_3\text{PO}_4/\text{Bi}_2\text{O}_3$ showed the strongest photocurrent signal among all of the as-prepared material. It is well known that light generated electrons and diffuses to the electrode surface lead to the photocurrent signal, and furthermore the

photoinduced holes are accepted in the electrolyte [45]. In general, the strongest current signal of $\text{GO-Ag}_3\text{PO}_4/\text{Bi}_2\text{O}_3$ explain the most efficient separation of the e^-/h^+ pairs and longest fluorescence lifetime of the photogenerated electron.

Role of the reactive species

The degradation mechanism of $\text{GO-Ag}_3\text{PO}_4/\text{Bi}_2\text{O}_3$ photocatalytic composite material was evaluated, the DMPO spin-trapping ESR and active species trapping experiments were investigated. As shown in Figure 9(a), there is no ESR signal in the dark. Under visible-light irradiation, the peaks of the $\text{DMPO}\cdot\text{O}_2^-$ radicals in $\text{GO-Ag}_3\text{PO}_4/\text{Bi}_2\text{O}_3$ are strong. After the introduction of GO, due to the dispersion of GO further improved electronic load migration, thus can be seen from the diagram $\text{DMPO}\cdot\text{O}_2^-$ the peaks are strongest. It is worth mentioning that the amount of $\bullet\text{O}_2^-$ radicals generated on the $\text{GO-Ag}_3\text{PO}_4/\text{Bi}_2\text{O}_3$. We speculate that the electrons in Ag_3PO_4 were transferred to GO, the e^- reacted with O_2 and generated $\bullet\text{O}_2^-$. The active species in $\text{GO-Ag}_3\text{PO}_4/\text{Bi}_2\text{O}_3$ were further studied during photocatalytic degradation. As can be seen from Figure 9(b), appear a small

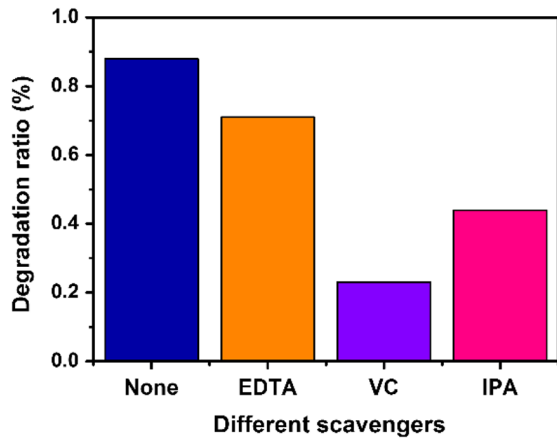


Figure 10. Comparison of photocatalytic activities of GO- $\text{Ag}_3\text{PO}_4/\text{Bi}_2\text{O}_3$ photocatalyst for the degradation of TC with or without adding EDTA, VC and IPA under visible light irradiation.

amount of DMPO- $\bullet\text{OH}$ peaks, the results show that a small amount of $\bullet\text{OH}$ radical is produced under the light irradiation. Because $\bullet\text{OH}$ was generated by the reaction between $\text{h}^+(\text{Bi}_2\text{O}_3)$ and OH^- .

The role of active species in the degradation process was further revealed over the GO- $\text{Ag}_3\text{PO}_4/\text{Bi}_2\text{O}_3$ photocatalytic composite material under visible-light irradiation, a variety of active species capture experiments were conducted by adjunction various trapping agents, for instance ammonium oxalate (EDTA) for h^+ , ascorbic acid (VC) for $\bullet\text{O}_2^-$ and isopropyl alcohol (IPA) for $\bullet\text{OH}$. The degradation ratio of TC over GO- $\text{Ag}_3\text{PO}_4/\text{Bi}_2\text{O}_3$ with different scavengers was shown in Figure 10. Compared with the degradation over GO- $\text{Ag}_3\text{PO}_4/\text{Bi}_2\text{O}_3$ without any scavengers, the photocatalytic activity of TC degradation after the addition of EDTA was not obvious affected. It indicates that h^+ have almost no influence in the photocatalytic reaction. Nevertheless, a significant inhibitory effect on photocatalytic activity was found when VC or IPA was added, especially, the degradation ratio of TC with the addition of VC is only

23%, suggesting the $\bullet\text{O}_2^-$ plays a significant role in the photocatalytic process. When IPA is added, the degradation ratios also is 56%, which indicates that $\bullet\text{OH}$ have limited effects in the photocatalytic reaction. The results of ESR analysis and active species trapping experiments indicated that the $\bullet\text{O}_2^-$ and $\bullet\text{OH}$ were the main active species. The trapping experiment result reveals that the electron conduction is supposed to follow a Z-scheme route.

Possible mechanism of the photocatalytic reaction process

The possible photocatalytic mechanism (Figure 11) was investigate to further understand the photodegradation systems. Under visible light irradiation, the phenomenon that electrons be excited and jumped from VB to CB appeared both in Ag_3PO_4 and Bi_2O_3 (Equations (1) and (2)). In the Z-scheme systems, the GO was employed as the electron acceptor and transport mediator which offers a place and pathway for the recombination of the holes in Ag_3PO_4 and electrons in Bi_2O_3 [28,46], resulting in high efficiency of the electron-hole separation in both two photocatalyst (Ag_3PO_4 and Bi_2O_3). The electrons in Ag_3PO_4 were transferred to GO (Equation (3)), the e^- reacted with O_2 and generated $\bullet\text{O}_2^-$ which can directly photodegrade TC into small molecules on the surface of GO (Equation (4)) [28,47,48], furthermore, $\bullet\text{OH}$ was generated by the reaction between $\text{h}^+(\text{Bi}_2\text{O}_3)$ and OH^- (Equation (5)). According to Figure 11, the $\bullet\text{O}_2^-$, $\bullet\text{OH}$ and h^+ were all active species which can react with TC and degrade it into small molecules (Equation (6)), and the specific reaction formula is as follows:

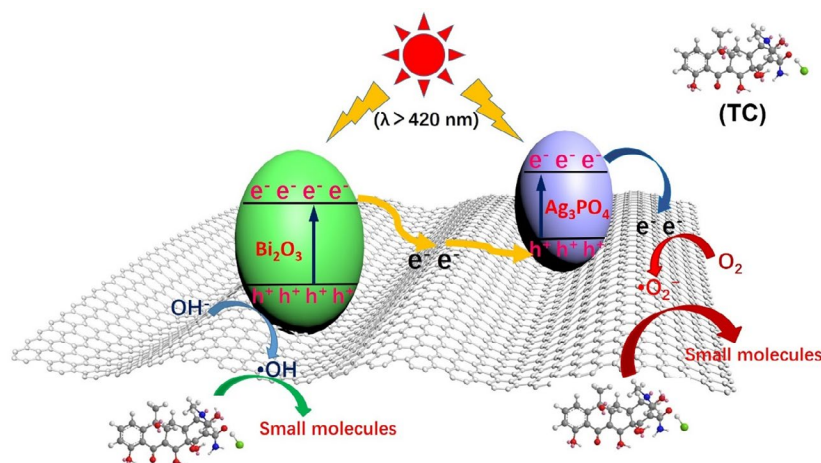
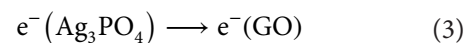
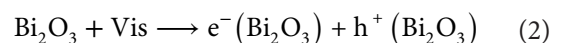
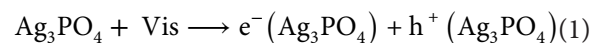
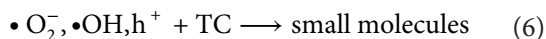
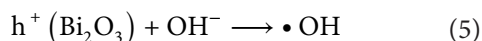
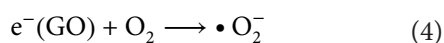


Figure 11. Proposed Z-scheme photocatalytic mechanism for GO- $\text{Ag}_3\text{PO}_4/\text{Bi}_2\text{O}_3$ photocatalytic complexes under visible-light illumination.



4. Conclusions

In this study, a series of GO-Ag₃PO₄/Bi₂O₃ photocatalytic complexes were successfully synthesized by a simple and efficiency method. Graphene oxide as a solid medium plays an important role in the construction of Z-scheme photocatalytic systems, GO is used to effectively transfer electrons from the conduction band Bi₂O₃ of to the valence band of Ag₃PO₄, promote the separation of photogenerated electrons and holes inspired by Ag₃PO₄ and Bi₂O₃, so as to improve the photocatalytic activity of this photocatalytic composite. The GO-Ag₃PO₄/Bi₂O₃ composite with the optimum Ag₃PO₄/Bi₂O₃ ratio (6:4) and amount ratio of GO (6 wt-%) exhibits a high photocatalytic TC degradation performance (88%) responding to visible light. According to the experimental results, the GO-multicomponent composites present higher photocatalytic activity than GO-singlecomponent, and GO as a solid medium has great potential in the construction of Z-scheme photocatalytic systems.

Disclosure statement

No potential conflict of interest was reported by the authors.

Funding

This work was supported by the National Natural Science Foundation of China [grant number 21676115] [grant number 21276116], [grant number 21477050], [grant number U1510126], [grant number U1662125] and [grant number 21407064], the Chinese-German Cooperation Research Project [grant number GZ1091], the Excellent Youth Foundation of Jiangsu Scientific Committee [grant number BK20140011], the Open Project of State Key Laboratory of Rare Earth Resource Utilizations [grant number RERU2014010], the Program for New Century Excellent Talents in University [grant number NCET-13-0835], the Henry Fok Education Foundation [grant number 141068] and Six Talents Peak Project in Jiangsu Province [grant number XCL-025].

References

- [1] Zhou M, Han D, Liu X, et al. Enhanced visible light photocatalytic activity of alkaline earth metal ions-doped CdSe/rGO photocatalysts synthesized by hydrothermal method. *Appl Catal B*. 2015;172:174–184.
- [2] Chandrasekaran S, Chung JS, Kim EJ, et al. Advanced nano-structured materials for photocatalytic water splitting. *J Electrochem Sci Tech*. 2016;7(1):1–12.
- [3] Chandrasekaran S, Hur SH, Choi WM, et al. Gold artichokes for enhanced photocatalysis. *Mater Lett*. 2015;160:92–95.
- [4] Zeng L, Lu Z, Li M, et al. A modular calcination method to prepare modified N-doped TiO₂ nanoparticle with high photocatalytic activity. *Appl Catal B*. 2016;183:308–316.
- [5] Huang G-F, Ma Z-L, Huang W-Q, et al. Ag₃PO₄ semiconductor photocatalyst: possibilities and challenges. *J Nanomater*. 2013;2013:8. Article ID 371356.
- [6] Tokunaga S, Kato H, Kudo A. Selective preparation of monoclinic and tetragonal BiVO₄ with scheelite structure and their photocatalytic properties. *Chem Mater*. 2001;13(12):4624–4628.
- [7] Taheri ME, Petala A, Frontistis Z, et al. Fast photocatalytic degradation of bisphenol A by Ag₃PO₄/TiO₂ composites under solar radiation. *Catal Today*. 2017;280:99–107.
- [8] Cao W, Gui Z, Chen L, et al. Facile synthesis of sulfate-doped Ag₃PO₄ with enhanced visible light photocatalytic activity. *Appl Catal B*. 2017;200:681–689.
- [9] Chandrasekaran S, Chung JS, Kim EJ, et al. Exploring complex structural evolution of graphene oxide/ZnO triangles and its impact on photoelectrochemical water splitting. *Chem Eng J*. 2016;290:465–476.
- [10] Chandrasekaran S, Kim EJ, Chung JS, et al. High performance bifunctional electrocatalytic activity of a reduced graphene oxide-molybdenum oxide hybrid catalyst. *J Mater Chem A*. 2016;4(34):13271–13279.
- [11] Chandrasekaran S, Choi WM, Chung JS, et al. 3D crumpled RGO-Co₃O₄ photocatalysts for UV-induced hydrogen evolution reaction. *Mater Lett*. 2014;136:118–121.
- [12] Perera SD, Mariano RG, Khiem V, et al. Hydrothermal synthesis of graphene-TiO₂ nanotube composites with enhanced photocatalytic activity. *ACS Catalysis*. 2012;2(6):949–956.
- [13] Mukherji A, Seger B, Lu GQ, et al. Nitrogen doped Sr₂Ta₂O₇ coupled with graphene sheets as photocatalysts for increased photocatalytic hydrogen production. *ACS Nano*. 2011;5(5):3483–3492.
- [14] Meng F, Li J, Cushing SK, et al. Photocatalytic water oxidation by hematite/reduced graphene oxide composites. *ACS Catalysis*. 2013;3(4):746–751.
- [15] Yang X, Cui H, Li Y, et al. Fabrication of Ag₃PO₄-graphene composites with highly efficient and stable visible light photocatalytic performance. *ACS Catalysis*. 2013;3(3):363–369.
- [16] Ding P, Du YG, Xu ZL. Effect of preparation methods of Bi₂O₃ nanoparticles on their photocatalytic activity. *Chem Res Chin Univ*. 2004;20(6):717–721.
- [17] Zhang L, Wang W, Yang J, et al. Sonochemical synthesis of nanocrystallite Bi₂O₃ as a visible-light-driven photocatalyst. *Appl Catal A*. 2006;308:105–110.
- [18] Wang C, Shao C, Wang L, et al. Electrospinning preparation, characterization and photocatalytic properties of Bi₂O₃ nanofibers. *J Colloid Interface Sci*. 2009;333(1):242–248.
- [19] Zhang Y, Guo Y, Fang B, et al. Continuously enhanced photoactivity of hierarchical beta-Bi₂O₃/Bi₂S₃ heterostructure derived from novel BiO₂CH₃ octagonal nanoplates. *Appl Catal A*. 2016;514:146–153.
- [20] Zhou P, Yu J, Jaroniec M. All-solid-state Z-scheme photocatalytic systems. *Adv Mater*. 2014;26(29):4920–4935.
- [21] Miyauchi M, Nukui Y, Atarashi D, et al. Selective growth of n-type nanoparticles on p-type semiconductors for Z-scheme photocatalysis. *ACS Appl Mater Interfaces*. 2013;5(19):9770–9776.

- [22] Yu W, Xu D, Peng T. Enhanced photocatalytic activity of g-C₃N₄ for selective CO₂ reduction to CH₃OH via facile coupling of ZnO: a direct Z-scheme mechanism. *J Mater Chem A*. 2015;3(39):19936–19947.
- [23] Zhang LJ, Li S, Liu BK, et al. Highly efficient CdS/WO₃ photocatalysts: Z-scheme photocatalytic mechanism for their enhanced photocatalytic H₂ evolution under visible light. *ACS Catalysis*. 2014;4(10):3724–3729.
- [24] Jin J, Yu J, Guo D, et al. A hierarchical Z-scheme CdS-WO₃ photocatalyst with enhanced CO₂ reduction activity. *Small*. 2015;11(39):5262–5271.
- [25] Shen H, Wang J, Jiang J, et al. All-solid-state Z-scheme system of RGO-Cu₂O/Bi₂O₃ for tetracycline degradation under visible-light irradiation. *Chem Eng J*. 2017;313:508–517.
- [26] Cui C, Wang Y, Liang D, et al. Photo-assisted synthesis of Ag₃PO₄/reduced graphene oxide/Ag heterostructure photocatalyst with enhanced photocatalytic activity and stability under visible light. *Appl Catal B*. 2014;158:150–160.
- [27] Shi Q, Zhao W, Xie L, et al. Enhanced visible-light driven photocatalytic mineralization of indoor toluene via a BiVO₄/reduced graphene oxide/Bi₂O₃ all-solid-state Z-scheme system. *J Alloy Compd*. 2016;662:108–117.
- [28] Xiang Q, Lang D, Shen T, et al. Graphene-modified nanosized Ag₃PO₄ photocatalysts for enhanced visible-light photocatalytic activity and stability. *Appl Catal B*. 2015;162:196–203.
- [29] Li J, Xie Y, Zhong Y, et al. Facile synthesis of Z-scheme Ag₂CO₃/Ag/AgBr ternary heterostructured nanorods with improved photostability and photoactivity. *J Mater Chem A*. 2015;3(10):5474–5481.
- [30] Dubale AA, Su W-N, Tamirat AG, et al. The synergistic effect of graphene on Cu₂O nanowire arrays as a highly efficient hydrogen evolution photocathode in water splitting. *J Mater Chem A*. 2014;2(43):18383–18397.
- [31] Chen G, Sun M, Wei Q, et al. Ag₃PO₄/graphene-oxide composite with remarkably enhanced visible-light-driven photocatalytic activity toward dyes in water. *J Hazard Mater*. 2013;244:86–93.
- [32] Xu Y-T, Guo Y, Li C, et al. Graphene oxide nano-sheets wrapped Cu₂O microspheres as improved performance anode materials for lithium ion batteries. *Nano Energy*. 2015;11:38–47.
- [33] Dong P, Wang Y, Cao B, et al. Ag₃PO₄/reduced graphene oxide sheets nanocomposites with highly enhanced visible light photocatalytic activity and stability. *Appl Catal B*. 2013;132:45–53.
- [34] Tan P, Chen X, Wu L, et al. Hierarchical flower-like SnSe₂ supported Ag₃PO₄ nanoparticles: Towards visible light driven photocatalyst with enhanced performance. *Appl Catal B*. 2017;202:326–334.
- [35] Pu Y-C, Lin W-H, Hsu Y-J. Modulation of charge carrier dynamics of Na_xH_{2-x}Ti₃O₇-Au-Cu₂O Z-scheme nanoheterostructures through size effect. *Appl Catal B*. 2015;163:343–351.
- [36] Zou W, Zhang L, Liu L, et al. Engineering the Cu₂O-reduced graphene oxide interface to enhance photocatalytic degradation of organic pollutants under visible light. *Appl Catal B*. 2016;181:495–503.
- [37] Liang Y, Lin S, Liu L, et al. Oil-in-water self-assembled Ag₂AgCl QDs sensitized Bi₂WO₆: Enhanced photocatalytic degradation under visible light irradiation. *Appl Catal B*. 2015;164:192–203.
- [38] Ohtsu N, Hiromoto S, Yamane M, et al. Chemical and crystallographic characterizations of hydroxyapatite- and octacalcium phosphate-coatings on magnesium synthesized by chemical solution deposition using XPS and XRD. *Surf Coat Technol*. 2013;218:114–118.
- [39] Wang C-Y, Zhang X, Qiu H-B, et al. Bi₂WO₆/Br₂ 10 nanosheets with controllable thickness for visible-light-driven catalytic degradation of tetracycline hydrochloride. *Appl Catal B*. 2017;205:615–623.
- [40] Zhao X, Lu Z, Wei M, et al. Synergistic effect of carbon sphere derived from yeast with magnetism and cobalt oxide nanochains towards improving photodegradation activity for various pollutants. *Appl Catal B*. 2018;220:137–147.
- [41] Jing LQ, Qu YC, Wang BQ, et al. Review of photoluminescence performance of nano-sized semiconductor materials and its relationships with photocatalytic activity. *Sol Energy Mater Sol Cells*. 2006;90(12):1773–1787.
- [42] Hou J, Yang C, Wang Z, et al. In situ synthesis of alpha-beta phase heterojunction on Bi₂O₃ nanowires with exceptional visible-light photocatalytic performance. *Appl Catal B*. 2013;142:504–511.
- [43] Li C, Chen G, Sun J, et al. A novel mesoporous single-crystal-like Bi₂WO₆ with enhanced photocatalytic activity for pollutants degradation and oxygen production. *ACS Appl Mater Interfaces*. 2015;7(46):25716–25724.
- [44] Xing W, Li C, Chen G, et al. Incorporating a novel metal-free interlayer into g-C₃N₄ framework for efficiency enhanced photocatalytic H₂ evolution activity. *Appl Catal B*. 2017;203:65–71.
- [45] Wu L, Li F, Xu Y, et al. Plasmon-induced photoelectrocatalytic activity of Au nanoparticles enhanced TiO₂ nanotube arrays electrodes for environmental remediation. *Appl Catal B*. 2015;164:217–224.
- [46] Wang P, Ao Y, Wang C, et al. A one-pot method for the preparation of graphene-Bi₂MoO₆ hybrid photocatalysts that are responsive to visible-light and have excellent photocatalytic activity in the degradation of organic pollutants. *Carbon*. 2012;50(14):5256–5264.
- [47] Han S, Hu L, Liang Z, et al. One-step hydrothermal synthesis of 2D hexagonal nanoplates of alpha-Fe₂O₃/graphene composites with enhanced photocatalytic activity. *Adv Func Mater*. 2014;24(36):5719–5727.
- [48] Zhang Y, Xie C, Gu FL, et al. Significant visible-light photocatalytic enhancement in Rhodamine B degradation of silver orthophosphate via the hybridization of N-doped graphene and poly(3-hexylthiophene). *J Hazard Mater*. 2016;315:23–34.